Journal of Organometallic Chemistry 895 (2019) 1–6

Contents lists available at ScienceDirect

Journal of Organometallic Chemistry

journal homepage: www.elsevier.com/locate/jorganchem

Luminescent [*fac*-Re(CO)$_3$-N∩O-phenylimidazole] complexes with parallel arrangement of twisted ligand motifs

Isha Mishra, Malaichamy Sathiyendiran*

School of Chemistry, University of Hyderabad, Hyderabad, 500046, India

ARTICLE INFO

Article history:
Received 27 March 2019
Received in revised form
10 May 2019
Accepted 13 May 2019
Available online 16 May 2019

Keywords:
2-(2′-hydroxyphenyl)benzimidazole
2-(2′-hydroxyphenyl)benzoxazole
2-(2′-hydroxyphenyl)benzothiazole
Phenylimidazole
Rhenium
Luminescence

ABSTRACT

Luminescent complexes [*fac*-Re(CO)$_3$(Y∩X)(ph-imz)] where (Y∩XH) = H$_2$-PBI = 2-(2′-hydroxyphenyl)-1*H*-benzimidazole, H-PB0 = 2-(2′-hydroxyphenyl)benzoxazole for **2**, and H-PBT = 2-(2′-hydroxyphenyl) benzothiazole for **3** and ph-imz = 2-phenylimidazole) were synthesized using Re$_2$(CO)$_{10}$, H$_2$-PBI/H-PBO/H-PBT and ph-imz *via* one-pot approach. All the three complexes were characterized using FT-IR, ^{1}H NMR, and single crystal X-ray diffraction analysis. The two coordinated, twisted ligand motifs are arranged closely parallel to each other and interacts through π···π stacking interactions in the solid state. The photophysical properties of the complexes were studied. All the complexes display moderate to strong emission both in the solution and solid state at room temperature.

1. Introduction

Tricarbonylrhenium(I)-based complexes possessing chelating N∩N units (2,2′-bipyridine (bpy), 1,10-phenanthroline and their derivatives) and monodentate neutral donors (pyridine, phosphine and their derivatives) have been gaining much interest in materials and biology [1–3]. The key properties associated with these complexes are kinetic inertness, photo-stability [4], and metal-to-ligand charge-transfer absorptions and emissions [5]. Research has been intensely focusing on the area to increase absorption and emission towards the red region. To achieve these properties, both chelating ligands and monodentate ligands are tuned by either introducing the substituted groups on the ligands or using structurally similar ligands like those of bpy but possessing different electronic properties [6]. In this category, 2-(2′-hydroxyphenyl)-1*H*-benzimidazole (H$_2$-PBI)/2-(2′-hydroxyphenyl)benzoxazole (H-PBO)/2-(2′-hydroxyphenyl)benzothiazole (H-PBT) are used to enhance the absorption in the visible region (350–450 nm). The complexes display emission at room temperature, both in solid and solution state. Recently, attempts have been made by incorporating nitrogen atom(s) in the anionic chelating ring and substituting various alkyl groups on the neutral monotopic nitrogen donor to enhance the photophysical properties [7]. The arrangement of these two ligand cores in the complexes is crucial for the solid state photophysical properties. The intra and inter molecular π···π stacking interactions between these two organic units in the complexes in the solid state play a significant role in photophysical properties. Up to now, tricarbonylrhenium(I) complexes with H$_2$-PBI/H-PBO/H-PBT motifs were centered on pyridine/pyridine derivatives. These complexes were synthesized using two steps synthetic approach [8a]. Attempt to use other monodentate heterocyclic donors like imidazole in place of pyridine motif in the complexes is also scarce. Similarly, one-step synthetic approach for the complexes, surprisingly, scarce [8]. Herein, we report three *fac*-Re(CO)$_3$-core based complexes [Re(CO)$_3$(Y∩X)L] ((Y∩XH)= HN-N∩O for **1**, O-N∩O for **2**, and S-N∩O for **3**) and L = 2-phenylimidazole) which were synthesized using Re$_2$(CO)$_{10}$, H$_2$-PBI/H-PBO/H-PBT and 2-phenylimidazole (ph-imz) *via* one-pot approach. Complexes **1**–**3** were characterized using various analytical and spectroscopic methods. The molecular structures of the complexes were determined using single crystal X-ray diffraction methods. The photophysical properties of the complexes were studied both in the solution and solid state.

* Corresponding author.
E-mail address: msathi@uohyd.ac.in (M. Sathiyendiran).

https://doi.org/10.1016/j.jorganchem.2019.05.014
0022-328X/

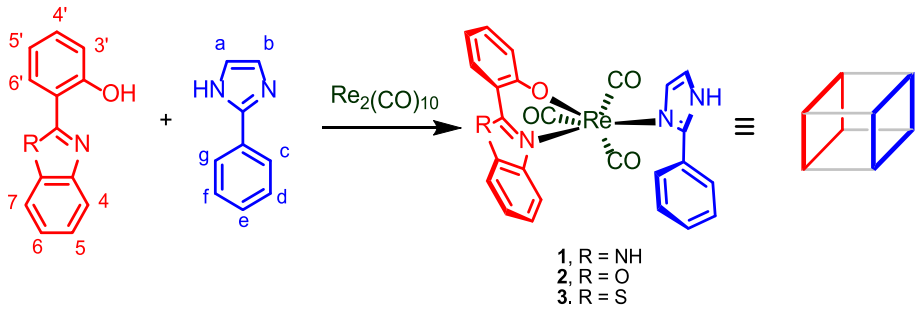

Scheme 1. Synthetic approach for **1**–**3**.

2. Results and discussion

2.1. synthesis of complexes *1*–*3*

The treatment of $Re_2(CO)_{10}$ with H_2-PBI/H-PBO/H-PBT and ph-imz in toluene resulted crystalline products **1**–**3** (Scheme 1). The complexes are air and moisture stable and soluble in polar organic solvents. The FT−IR spectra of the complexes display three carbonyl stretching bands in the range 2014–1856 cm^{-1}, corresponding to the *fac*-tricarbonyl rhenium (I) motif [9a]. The ^1H NMR spectrum of complex **3** in DMSO-d_6 shows two types of pattern which are assigned using $^1H-^1H$ COSY spectroscopic methods. The presence of two sets of peaks may be considered to correspond for major and minor isomers due to the rotation of the phenyl ring in ph-imz motif in solution. In particular, triplet and doublet were observed for the protons ($H^{3'-6'}$ and $H^{4,7}$) in the high-field region (Electronic supporting information, ESI Fig. S1–S3). The data clearly indicates that moderate to strong intramolecular interactions exist between the two aromatic ligand motifs. A similar kind of pattern was observed for complexes **1** and **2**.

2.2. molecular structures of complexes *1*–*3*

Molecular structures of **1**–**3** were determined using single crystal X-ray diffraction analysis. The geometry around the rhenium core, and the arrangement of two organic ligands in the complexes are similar to each other. The rhenium is in distorted octahedral geometry in the complexes. Two chelating atoms (N∩O atoms) and two carbonyl carbon atoms are in the square planar geometry. The axial position of octahedral geometry is occupied by N from imidazole and one carbonyl carbon. The Re−O(PBI)/Re−N (ph-imz) distance is 2.137(5)/2.203(6) Å for **1**, 2.167(3)/2.214(3) Å for **2**, 2.209(4)/2.202(4) Å for **3**, which indicate the ionic/coordination interactions between these two atoms. The Re−N (ph-imz) distance is 2.202–2.214 Å, which is in the expected range for Re−N (neutral heterocyclic donor) [8–11]. It is noteworthy to discuss the arrangement of the two organic donors in the complexes. Though the stoichiometry and bonding parameters of **1**–**3** are very similar to the complexes reported previously [8a], the two organic units are twisted significantly in **1**–**3** resulting in the intramolecular π•••π stacking interactions (Fig. 1). Though N∩O atoms are in the square plane, the benzimidazole as well as phenolate motifs are not in the square plane. The phenolate is above the square plane whereas benzimidazole is below to it. The Re−N (imidazolyl) bond is bent towards chelating unit. In particular, the imidazolyl unit is bent with respect to Re−N plane. The dihedral angle between the phenolate and the imidazole is (10.14° in **1**, 5.06° in **2** and 6.81° in **3**). A similar kind of arrangement is found in those complexes possessing imidazole and phenanthroline units [11]. In general, the phenyl unit and imidazole unit in 2-phenylimidazole are twisted with respect to each other to avoid steric repulsion (H•••H) [12]. The phenyl unit of ph-imz is positioned over the chelating unit in **1**–**3** with the distance of 3.6 Å (centre of mass, $COM_{ph}\cdots COM_{NS/NO}$), which indicates the strong π•••π stacking interactions between these units. The intramolecular interactions found between these units are slipped co-facial π•••π stacking interactions (Fig. 1, ESI Tables S2b, S3b and S4b). It is important to mention that the *fac*-$Re(CO)_3$ core based complex (**I**) containing 8-hydroxyquinolate and 2-phenylimidazole motifs was recently reported by Tseng et al. [8d] The dihedral angle between the 8-hydroxyquinolate and imidazole/phenyl is 77.6/19° in **I**. The moderate intramolecular π•••π stacking interactions were found between the edge of pyridine unit of the 8-hydroxyquinolate and the edge of the phenyl motif of ph-imz in complex **I** [8d].

Intermolecular interactions. In the crystal lattice of complex **1**–**3**, each molecule is involved in intermolecular N−H···O hydrogen bonding interactions between the imidazole N−H groups and the metal coordinated O atoms of the phenolate motif in the chelating unit. The N•••O distances are in the range 2.697–2.742 Å and the N−H···O angles are within range 170°–176°. In each case, self-assembly of the complexes through intermolecular N−H···O hydrogen bonds result in the formation of a one dimensional chain (ESI Fig. S4). Complex **2** and **3** are further stabilized by intermolecular C−H•••π interactions between the two adjacent molecules (imidazole unit to benzoxazole/benzothiazole unit, dihedral angle = 54°/64°, distance = 5.049/5.296 Å) (ESI Tables S3c and S4c). However, these kinds of interactions are not observed for **1**. H_2-PBI/H-PBO/H-PBT based $Re(CO)_3$ complexes with pyridine/pyridine derivatives adapt the structure in which the N∩O chelating ligand and pyridyl unit are arranged orthogonally [8]. In the complexes **1**–**3**, though the imidazole unit is similar to pyridyl unit, based on the structure and coordinating ability, the presence of phenyl in ph-imz motif alter the arrangement of these two units. In the complexes, the H_2-PBI/H-PBO/H-PBT and ph-imz ligand motifs are twisted significantly, thereby, lying closely parallel to each other.

2.3. photophysical studies of *1*–*3*

The absorption properties of complexes **1**–**3** were studied both in dichloromethane (DCM) and dimethylsulfoxide (DMSO) at room temperature (Fig. 2, Table 1, and ESI Fig. S5). The UV−Vis spectra of **1**–**3** in DCM closely match with those of **1**–**3** in DMSO. The intense absorptions in the range of 200–350 nm can be assigned to predominantly ligand-based electronic transitions (π−π* including N∩X ® N∩X and N∩X ® ph-imz) (ESI Fig. S5). The higher energy absorption (~300–350 nm) may also contain significant amount of MLCT electronic transitions (Re → N∩XRe → N∩X) [9a]. The moderate absorptions in the visible region of 350–500 nm can be attributed to the metal-to-ligand charge-transfer (MLCT) electronic transitions with small contribution of intraligand charge-transfer (ILCT) electronic transitions [10a].

All the complexes display emission both in solution and solid

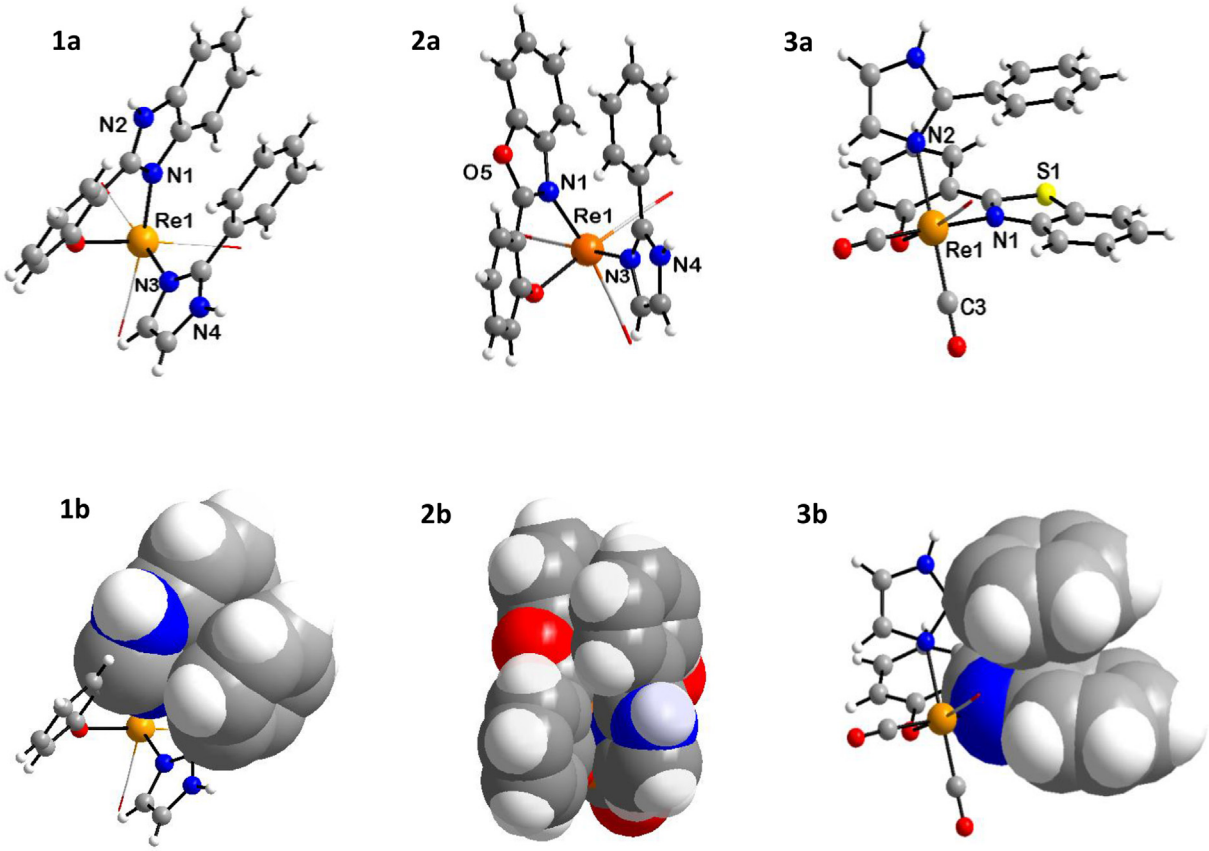

Fig. 1. Molecular structures of **1**–**3**, ball and stick (1a-3a) and space-fill model (1b-3b) showing π···π stacking interactions. (C = gray, H = white, N = blue, O = red, S = yellow, Re = orange). (For interpretation of the references to colour in this figure legend, the reader is referred to the Web version of this article.)

state. The emission properties of the complexes in DCM/DMSO were studied with and without nitrogen purged solution (Table 1, Fig. 3–5, ESI Fig. S6-S18). Complex **1** displayed poorly structured emission band in DCM (ESI Fig. S6). The emission intensity of **1** is slightly enhanced in nitrogen purged solution with red shift by 4 nm (ESI Fig. S7). Excitation spectrum of **1** at 516 nm displayed three structured bands below 350 nm (ESI Fig. S8). The broad band with maximum at 388 nm for **1** in the UV-Vis absorption spectrum is absent in the excitation spectrum of **1**. The emission of **1** from the ^{1}MLCT/^{3}MLCT excited state is omitted/less because the main absorption maxima for MLCT electronic transition is absent in the excited state spectrum. The results indicate that the emission of **1** in DCM is mainly originated from the ligand centered (LC) excited state or intra ligand centered (IL) excited state. The emission spectrum of **1** in DMSO showed structured emissions which are blue shifted by 40 nm compared to those emission in DCM. The excitation spectrum of **1** in DMSO at 476 nm displayed bands similar to those of **1** in DCM except intensities. This can be explained that the emission of **1** in DMSO is also originated from the LC or IL excited states. However, the population of these two excited states is reversed in DMSO as compared to those in DCM. The blue shifted emission of **1** in DMSO by 40 nm may be due to rigidochromic effect [13]. The solvent DMSO molecules may interact with ligand motifs of **1** through hydrogen bonding interactions [N–H···O=S(CH$_3$)$_2$] which provides rigidity to the ligand centered excited state [14].

Single crystal/powder **1** displays well-structured emission spectrum, which is red-shifted as compared to that in DCM/DMSO (Fig. 3). It is noteworthy to mention that the free H$_2$-PBI in solid state displays poorly structured emission with emission maximum of 443/470 nm [15]. The results clearly indicates that crystal **1** emits from three different excited states which may be assigned as LC-, ^{3}MLCT-, and metal-to-ligand-ligand charge transfer (^{3}MLLCT) excited states [16]. The slipped co-facial π•••π stacking interactions caused due to conformational rotation of phenyl motif in phenylimidazolyl ligand in the complexes plays a major role for the red-shifted emission in the solid state. A similar kind of red-shifted emission was observed in helicate containing Re(CO)$_3$ core, anionic PBI motif, and benzimidazolyl core [9a]. Closely looking the crystal structure of **1** indicates that two neighbouring PBI motifs interact each other through weak π···π stacking interactions (ESI Table S2c).

Compound **2** in DCM/DMSO is emissive (Fig. 4, ESI Fig. S9/S15). Similar to the absorption spectrum, the emission maximum of **2** in solution is red shifted as compared to complex **1** (Fig. 4, ESI Fig. S6). No significant shift in the emission pattern as well as life-time data of **2** was observed while changing solvent from DCM to DMSO. Crystal **2** displays poorly resolved emission pattern (Fig. 5). The emission pattern is different from that of crystal **1**. The emission of **2** is red-shifted as compared to crystal of H-PBO (free ligand) [17].

The emission pattern of **3** in DCM is almost similar to that in DMSO. Complex **3** displays broad emission, the emission maximum is red-shifted as compared to **1** and **2** in DMSO and DCM (Fig. 4, ESI Fig. S6). The life-time data of complex **2** and **3** were studied both in DCM and DMSO and were found to be similar (Table 2, ESI Fig. S19–S22). The emission decays of both complexes are biexponential. From the data, it can be inferred that the complexes emit from two different excited states denoted by τ_1 and τ_2 (Table 2). Similar emission decays with shorter lifetime were observed for other rhenium complexes [9].

In addition, the crystal emission of **3** is identical to that of crystal

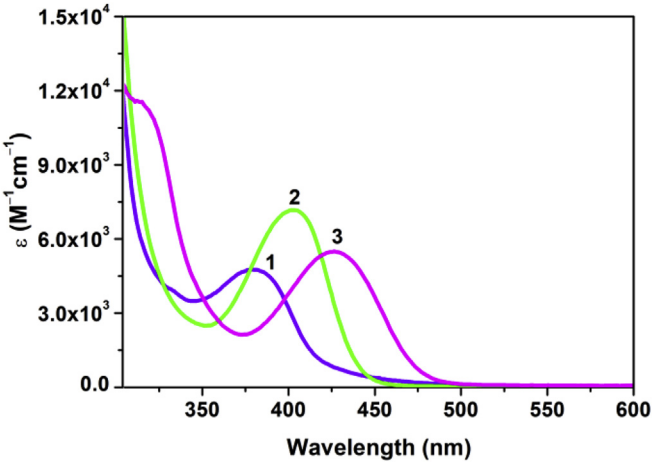

Fig. 2. Absorption spectra of **1**–**3** in DMSO.

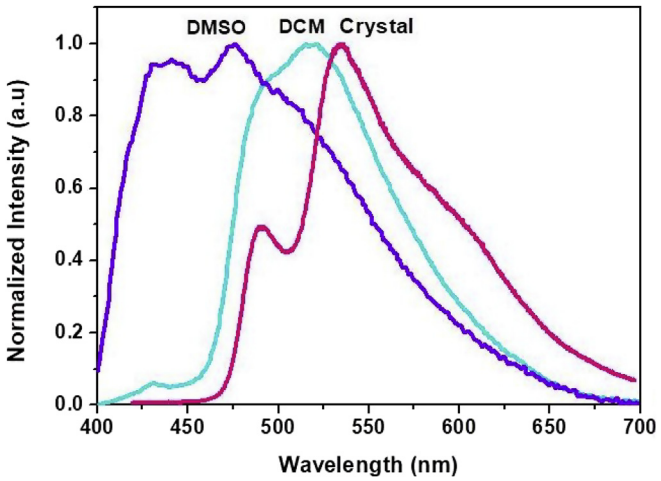

Fig. 3. Emission spectra of **1** in DMSO, DCM, and crystal (solid state).

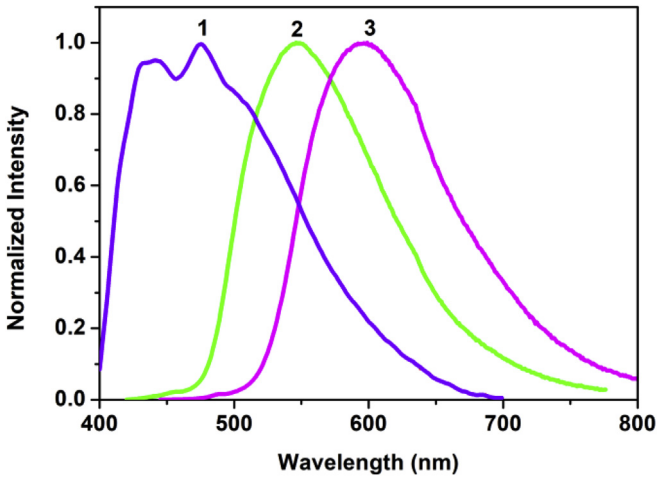

Fig. 4. Emission spectra of **1**–**3** in DMSO.

2 (Fig. 5). The results reveals that complexes **2** and **3** display emission which may be originated from the ^{3}MLCT and ^{3}MLLCT excited states because changing the anionic unit in the complexes from H-PBO to H-PBT did not alter the emission pattern in the solid-state. It is noteworthy to mention that the photophysical properties of complexes with similar anionic ligands (HPBI/PBO/PBT) but different neutral donor (pyridine) at low temperature (77 K) are blue shifted [8a]. However, the complexes **1**–**3** shows red shifted emission in the solid state. The results clearly indicate that tuning of the coordinating donor motif can shift the emission properties towards the red region.

3. Conclusion

The three luminescent heteroleptic mononuclear *fac*-Re(CO)$_3$ core containing complexes were synthesized using H_2-PBI/H-PBO/H-PBT, 2-phenylimidazole and $Re_2(CO)_{10}$ *via* one pot synthetic approach. The molecular structures of the complexes indicated the parallel arrangement of the two organic motifs which are coordinated to metal core and twisted significantly, resulting in slipped co-facial $\pi\cdots\pi$ interactions between the phenyl unit of ph-imz and benzimidazolyl of chelating motif in solid state. The photo physical properties of the complexes display strong emission both in the solution and solid state at room temperature. The synthesis of various acyclic and cyclic Re(I) based complexes using different nitrogen donors (phenyl benzimidazole/phenylnaphthyl benzimidazole) is under progress.

4. Materials and methods

4.1. General data

Starting materials such as $Re_2(CO)_{10}$, 2-(2′-hydroxyphenyl) benzoxazole (H-PBO), 2-(2′-hydroxyphenyl)benzothiazole (H-PBT), 2-phenylimidazole (ph-imz), toluene and spectroscopic grade solvents such as dimethylsulfoxide (DMSO, Finar), dichloromethane (DCM, Finar) were obtained from commercial sources and used as received. 2-(2′-hydroxyphenyl)-1*H*-benzimidazole (H_2-PBI) was synthesized by previously reported method [7a]. Elemental analyses were performed on Flash EA 1112 series CHNS analyser. FT-IR spectra were recorded on a Nicolet iS5 FT-IR spectrometer. NMR spectra were recorded on Bruker Avance III 400 and 500 MHz instruments. Absorption spectra were recorded on UV-3600 Shimadzu UV–Vis–NIR spectrophotometer. Fluorescence spectra were measured on Horiba FluoroMax 4 fluorimeter. Solid State

Table 1
Absorption and Emission data for **1**–**3** in solution and solid state (Crystal).

	λ^{abs}_{max}, nm (ε, M^{-1} cm^{-1})	λ^{em}_{max} (λ^{ex}_{max}) nm		ϕ_{em}
	DMSO	DMSO	crystal	
H_2-PBI [15]		464 (320, 334)	443 (350)	–
1	290 (19641) 382 (4831)	440, 474 (380)	535 (405)	–
H-PBO [17]		370	481 (320)	–
2	292 (28607) 403 (7240)	547 (400)	556 (405)	0.0212 ± 0.0007
H-PBT [18]			525 (345)	–
3	315 (11598) 426 (5576)	594 (425)	556 (405)	0.019 ± 0.003

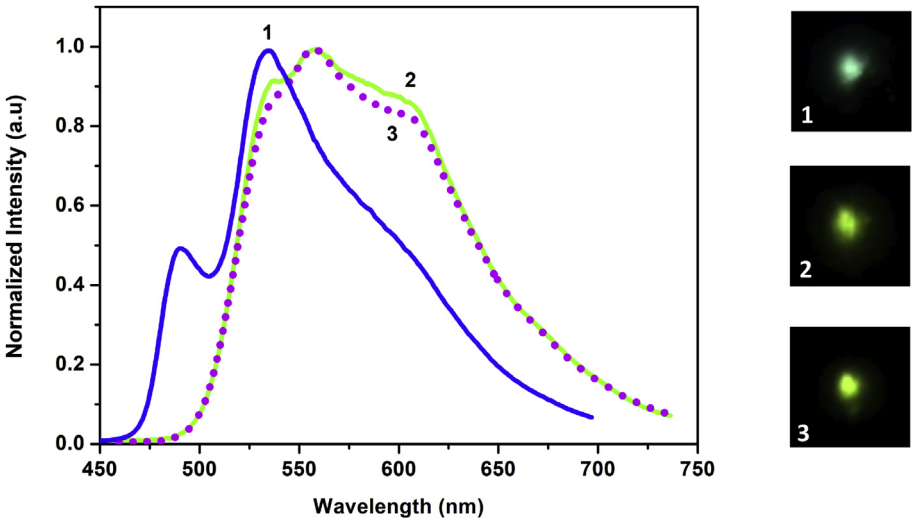

Fig. 5. Normalized emission spectra of **1-3** in solid state (crystal) at room temperature ($\lambda_{ex} = 405$ nm). Right: Photograph of the emission under irradiation from a 405 nm excitation source.

Table 2
Emission lifetime (τ, ns) of **2** and **3** in solution.

Complex	Solvent	λ_{mon}	τ_1	τ_2	χ^2
2	DCM	526	10670	1160	0.99
	DMSO	526	1730	11890	0.99
3	DCM	572	1730	11890	0.99
	DMSO	576	1730	11890	0.99

λ_{mon} = monitoring wavelength, τ = lifetime for each component, χ^2 = indicating the goodness of the fit to the data.

emission spectra were recorded on WI-Tec confocal Raman spectrometer with 405 nm as the excitation source. The lifetime of the complexes was measured using a time-correlated single-photon counting (TCSPC) fluorescence spectrometer (Horiba JobinYvon IBH). The relative quantum yield for the complexes was calculated using $[Ru(bpy)_3](PF_6)_2$ as standard in acetonitrile solution. The formula used for the calculation is as follows: $f_S/f_R = (n_S/n_R)^2 (m_S/m_R)$, f: Quantum yield efficiency m: Slope of the line obtained from integrated fluorescence intensity vs absorbance plot. n: Refractive index of the respective solvents. Subscript R refers to the reference of known quantum yield and S refers to the sample [19].

*General Synthetic Approach for **1**–**3**.* $Re_2(CO)_{10}$, 2-(2′-hydroxyphenyl)-1*H*-benzimidazole (H_2-PBI)/2-(2′-hydroxyphenyl) benzoxazole (H-PBO)/2-(2′-hydroxyphenyl)benzothiazole (H-PBT) and 2-phenylimidazole (ph-imz) in toluene (~10 mL) were kept in a Teflon vessel. The vessel was kept in the stainless steel solvothermal bomb and placed in an oven programmed at 160 °C for 48 h and cooled to room temperature. Crystals or powder obtained in the bomb were filtered, washed with hexane, and air dried.

4.2. Synthesis of [$Re(CO)_3$(H_2-PBI) (ph-imz)] **(1)**

Yellow coloured needle shaped crystals were obtained using $Re_2(CO)_{10}$ (100.5 mg, 0.154 mmol), H_2-PBI (64.4 mg, 0.306 mmol) and ph-imz (44.1 mg, 0.306 mmol) in toluene (~10 mL). Yield: 51% (48.5 mg). Anal. Calcd. For $C_{25}H_{17}N_4O_4Re$: C, 48.15; H, 2.75; N, 8.98. Found: C, 48.23; H, 2.72; N, 8.91. FT-IR (ν_{max} (KBr)/cm^{-1}) 2009, 1864 (CO). ^{1}H NMR (400 MHz, DMSO-d_6): δ 7.94–7.91 (m, 3H, $H^{g,c,7}$), 7.80 (dd, 1H, $J = 8$ Hz, $H^{6'}$), 7.60–7.58 (m, 1H, H^4), 7.44 (t, 3H, $J = 7$ Hz, $H^{f,d}$), 7.39–7.23 (m, 6H, $H^{a,b,e,4'}$), 7.14 (s, 2H, $H^{5,6}$), 6.82 (dd, 1H, $J = 8.4$ Hz, $H^{3'}$), 6.70–6.66 (m, 1H, $H^{5'}$).

4.3. Synthesis of [$Re(CO)_3$(H-PBO) (ph-imz)] **(2)**

Brown coloured needle shaped crystals were obtained using $Re_2(CO)_{10}$ (100.4 mg, 0.154 mmol), H-PBO (65.1 mg, 0.307 mmol) and ph-imz (44.1 mg, 0.306 mmol) in toluene (~10 mL). Yield: 32% (30.4 mg). Anal. Calcd. For $C_{25}H_{16}N_3O_5Re$: C, 48.07; H, 2.58; N, 6.73. Found: C, 48.15; H, 2.52; N, 6.68. FT-IR (ν_{max} (KBr)/cm^{-1}) 2012, 1902 and 1866 (CO). ^{1}H NMR (500 MHz, DMSO-d_6): δ 7.95–7.92 (m, 3H, $H^{g,c,7}$), 7.89 (d, $J = 8$ Hz, 1H, H^4), 7.74 (dd, $J = 8$ Hz, 1H, $H^{6'}$), 7.62–7.53 (m, 2H, $H^{6,4'}$), 7.46–7.43 (m, 3H, $H^{f,d}$), 7.41–7.37 (m, 1H, H^5), 7.35–7.32 (m, 2H, H^e), 7.22–7.15 (m, 3H, $H^{a,b}$), 6.90–6.86 (m, 2H, $H^{3'}$), 6.77–6.70 (m, 2H, $H^{5'}$).

4.4. Synthesis of [$Re(CO)_3$(H-PBT) (ph-imz)] **(3)**

Yellow coloured crystals were obtained using $Re_2(CO)_{10}$ (100.6 mg, 0.154 mmol), H-PBT (70.1 mg, 0.307 mmol) and ph-imz (44.2 mg, 0.307 mmol) in toluene (~10 mL). Yield: 31% (30.2 mg). Anal. Calcd. For $C_{25}H_{16}N_3O_4ReS$: C, 46.87; H, 2.52; N, 6.56, S, 5.00. Found: C, 46.79; H, 2.56; N, 6.51, S, 4.92. FT-IR (ν_{max} (KBr)/cm^{-1}) 2013, 1904 and 1864 (CO). ^{1}H NMR (500 MHz, DMSO-d_6): δ 8.30 (d, 1H, $J = 8.5$ Hz, H^7), 8.19 (dd, 1H, $J = 8$ Hz, H^4), 7.94 (dd, 2H, $J = 8.5$ Hz, $H^{g,c}$), 7.73–7.68 (m, 2H, $H^{5',5}$), 7.54–7.53 (m, 3H, $H^{f,d,6}$), 7.39–7.33 (m, 4H, $H^{e,6'}$), 7.23 (s, 2H, $H^{a,b}$), 6.86–6.83 (m, 1H, $H^{3'}$), 6.70–6.67 (m, 1H, $H^{4'}$).

4.5. X-ray crystal data for complexes **1**–**3**

Crystallography intensity data of crystals of **1**–**3** were collected on a Bruker D8 QUEST diffractometer [λ(Mo Kα) = 0.71073 Å]. The structures were solved by direct methods using SHELXS-97 [20a] and refined using the SHELXL-2018/3 program (within the WinGX program package) [20b,c]. Non-H atoms were refined anisotropically. The crystallographic data of **1**–**3** are provided in ESI Tables S1–S4c. The crystallographic data for **1** shows higher value of R^{int} due to poor crystal quality.

Acknowledgements

We thank University of Hyderabad and DST-SERB (EMR/2015/000627) for facilities and funding. IM thanks DST for DST-INSPIRE.

Appendix A. Supplementary data

Supplementary data to this article can be found online at https://doi.org/10.1016/j.jorganchem.2019.05.014.

References

[1] (a) X. Gong, P.K. Ng, W.K. Chan, Adv. Mater. 10 (1998) 1337–1340;
(b) X. Liu, H. Xia, W. Gao, Q. Wu, X. Fan, Y. Mu, C. Ma, J. Mater. Chem. 22 (2012) 3485–3492;
(c) A. Kastl, S. Dieckmann, K. Wahler, T. Volker, L. Kastl, A.L. Merkel, A. Vultur, B. Shannan, K. Harms, M. Ocker, W.J. Parak, M. Herlyn, E. Meggers, ChemMedChem 8 (2013) 924–927;
(d) T.M. McLean, J.L. Moody, M.R. Waterland, S.G. Telfer, Inorg. Chem. 51 (2012) 446–455.

[2] (a) S. Ranjan, S.Y. Lin, K.C. Hwang, Y. Chi, W.L. Ching, C.S. Liu, Y.T. Tao, C.H. Chien, S.M. Peng, G.H. Lee, Inorg. Chem. 42 (2003) 1248–1255;
(b) T. Klemens, A. Świtlicka-Olszewska, B. Machura, M. Grucela, E. Schab-Balcerzak, K. Smolarek, S. Mackowski, A. Szlapa, S. Kula, S. Krompiec, P. Lodowski, A. Chrobok, Dalton Trans. 45 (2016) 1746–1762.

[3] (a) H. Tsubaki, A. Sekine, Y. Ohashi, K. Koike, H. Takeda, O. Ishitani, J. Am. Chem. Soc. 127 (2005) 15544–15555;
(b) T. Morimoto, C. Nishiura, M. Tanaka, J. Rohacova, Y. Nakagawa, Y. Funada, K. Koike, Y. Yamamoto, S. Shishido, T. Kojima, T. Saeki, T. Ozeki, O. Ishitani, J. Am. Chem. Soc. 135 (2013) 13266–13269;
(c) W.K. Chu, C.C. Ko, K.C. Chan, S.M. Yiu, F.L. Wong, C.S. Lee, V.A.L. Roy, Chem. Mater. 26 (2014) 2544–2550.

[4] (a) A.J. Amoroso, M.P. Coogan, J.E. Dunne, V. Fernandez-Moreira, J.B. Hess, A.J. Hayes, D. Lloyd, C. Millet, S.J.A. Pope, C. Williams, Chem. Commun. (2007) 3066–3068;
(b) V. Fernandez-Moreira, F.L. Thorp-Greenwood, M.P. Coogan, Chem. Commun. 46 (2010) 186–202;
(c) S. Clede, F. Lambert, C. Sandt, Z. Gueroui, M. Refregiers, M. Plamont, P. Dumas, A. Vessieres, C. Policar, Chem. Commun. 48 (2012) 7729–7731.

[5] (a) M. Wrighton, D.L. Morse, J. Am. Chem. Soc. 96 (1974) 998–1003;
(b) L. Sacksteder, A.P. Zipp, E.A. Brown, J. Streich, J.N. Demás, B.A. DeGraff, Inorg. Chem. 29 (1990) 4335–4340;
(c) A.J. Lees, Chem. Rev. 87 (1987) 711–743;
(d) D.J. Stufkens, A. Vlcek Jr., Coord. Chem. Rev. 177 (1998) 127–179;
(e) A. Gabrielsson, M. Busby, P. Matousek, M. Towrie, E. Hevia, L. Cuesta, J. Perez, S. Zalis, A. Vlcek Jr, Inorg. Chem. 45 (2006) 9789–9797.

[6] (a) S.L. Huang, T.S.A. Hor, G.X. Jin, Coord. Chem. Rev. 333 (2017) 1–26;
(b) H.N. Zhang, W.X. Gao, Y.X. Deng, Y.J. Lin, G.X. Jin, Chem. Commun. 54 (2018) 1559–1562.

[7] (a) X. Han, H. Ma, Y. Wang, Russ. J. Org. Chem. 44 (2008) 863–865;
(b) C. Wu, S. Tao, M. Chen, F.L. Wong, Y. Yuan, H.W. Mo, W. Zhao, C.S. Lee, Chem. Asian J. 8 (2013) 2575–2578;
(c) Z. Zhang, H. Zhang, C. Jiao, K. Ye, H. Zhang, J. Zhang, Y. Wang, Inorg. Chem. 54 (2015) 2652–2659.

[8] (a) R. Czerwieniec, A. Kapturkiewicz, R.A. Ostrowska, J. Nowacki, J. Chem. Soc., Dalton Trans. (2002) 3434–3441;
(b) C.C. Ju, A.G. Zhang, H.L. Sun, K.Z. Wang, W.L. Jiang, Z.Q. Bian, C.H. Huang, Organometallics 30 (2011) 712–716;
(c) Y.Y. Lu, C.C. Ju, D. Guo, Z.B. Deng, K.Z. Wang, J. Phys. Chem. C 111 (2007) 5211–5217;
(d) T.W. Tseng, S. Mendiratta, T.T. Luo, T.W. Chen, Y.P. Lee, Inorg. Chim. Acta 477 (2018) 312–317.

[9] (a) B. Shankar, S. Sahu, N. Deibel, D. Schweinfurth, B. Sarkar, P. Elumalai, D. Gupta, F. Hussain, G. Krishnamoorthy, M. Sathiyendiran, Inorg. Chem. 53 (2014) 922–930;
(b) A.E. Nahhas, C. Consani, A.M. Blanco-Rodríguez, K.M. Lancaster, O. Braem, A. Cannizzo, M. Towrie, I.P. Clark, S. Zalis, M. Chergui, A. Vlcek Jr., Inorg. Chem. 50 (2011) 2932–2943;
(c) J. Skiba, A. Kowalczyk, P. Staczek, T. Bernas, D. Trzybinski, K. Wozniak, U. Schatzschneider, R. Czerwieniec, K. Kowalski, New J. Chem. 43 (2019) 573–583.

[10] (a) B. Shankar, P. Elumalai, M. Sathiyendiran, Inorg. Chem. Commun. 36 (2013) 109–112;
(b) S.K. Behera, G. Sadhuragiri, P. Elumalai, M. Sathiyendiran, G. Krishnamoorthy, RSC Adv. 6 (2016) 59708–59717;
(c) P. Saxena, B. Shankar, M. Sathiyendiran, J. Organomet. Chem. 799–800 (2015) 82–89.

[11] (a) M. Fumanal, E. Gindensperger, C. Daniel, Phys. Chem. Chem. Phys. 20 (2018) 1134–1141;
(b) M. Fumanal, C. Daniel, J. Comput. Chem. 37 (2016) 2454–2466.

[12] (a) A. Mukhopadhyay, S. Pal, Eur. J. Inorg. Chem. (2006) 4879–4887;
(b) M. Lousame, A. Fernandez, M. Lopez-Torres, D. Vazquez-Garcıa, J.M. Vila, A. Suarez, J.M. Ortigueira, J.J. Fernandez, Eur. J. Inorg. Chem. (2000) 2055–2062.

[13] (a) M.K. Itokazu, A.S. Polo, N.Y.M. Iha, J. Photochem. and Photobiol. A: Chem. 160 (2003) 27–32;
(b) T.G. Kotch, A.J. Lees, S.J. Fuerniss, K.I. Papathomas, R.W. Snyder, Inorg. Chem. 32 (1993) 2570–2575.

[14] (a) J. Zukerman-Schpector, E.R.T. Tiekink, CrystEngComm 16 (2014) 6398–6407;
(b) O.K. Abou-Zied, R. Jimenez, E.H.Z. Thompson, D.P. Millar, F.E. Romesberg, J. Phys. Chem. A 106 (2002) 3665–3672.

[15] (a) T. Shida, T. Mutai, K. Araki, CrystEngComm 15 (2013) 10179–10182;
(b) H. Konoshima, S. Nagao, I. Kiyota, K. Amimoto, N. Yamamoto, M. Sekine, M. Nakata, K. Furukawa, H. Sekiya, Phys. Chem. Chem. Phys. 14 (2012) 16448–16457.

[16] (a) Y.J. Cho, S.Y. Kim, M. Cho, K.R. Wee, H.J. Son, W.S. Han, D.W. Cho, S.O. Kang, Phys. Chem. Chem. Phys. 18 (2016) 15162–15169;
(b) K.K.W. Lo, K.Y. Zhang, S.K. Leung, M.C. Tang, Angew. Chem. Int. Ed. 47 (2008) 2213–2216.

[17] (a) F.S. Rodembusch, F.R. Brand, D.S. Correa, J.C. Pocos, M. Martinelli, V. Stefani, Mater. Chem. Phys. 92 (2005) 389–393;
(b) J.E. Kwon, S.Y. Park, Adv. Mater. 23 (2011) 3615–3642.

[18] P. Majumdar, J. Zhao, J. Phys. Chem. B 119 (2015) 2384–2394.

[19] [a] J.R. Lakowicz, Principles of Fluorescence Spectroscopy, Springer, 2006;
[b] A.M. Brouwer, Pure Appl. Chem. 83 (2011) 2213–2228.

[20] (a) G.M. Sheldrick, Program for Crystal Structure Solution. SHELXS-97, University of Göttingen, Göttingen, Germany, 1997;
(b) G.M. Sheldrick, ActaCrystallogr., Sect. A: Found. Crystallogr. 64 (2008) 112–122;
(c) G.M. Sheldrick, ActaCrystallogr., Sect. C: Struct. Chem. 71 (2015) 3–8.